A new type of quantum speed meter interferometer: How measuring speed can help to observe black holes.

Stefan L. Danilishin,[1,2,*] Eugene Knyazev,[3] Nikita V. Voronchev,[3] Farid Ya. Khalili,[3] Christian Gräf,[1] Sebastian Steinlechner,[4] Jan-Simon Hennig,[1] and Stefan Hild[1]

[1]*SUPA, School of Physics and Astronomy, University of Glasgow, Glasgow G12 8QQ, United Kingdom*
[2]*Institut für Theoretische Physik, Leibniz Universität Hannover and Max-Planck Institut für Gravitationsphysik (Albert-Einstein-Institut), Callinstrae 38, D-30167 Hannover, Germany*
[3]*M.V. Lomonosov Moscow State University, Faculty of Physics, Moscow 119991, Russia*
[4]*Institut für Laserphysik und Zentrum für Optische Quantentechnologien der Universität Hamburg, Luruper Chaussee 149, 22761 Hamburg, Germany*

[illegible] $^2 - 10^3 M_\odot$ [illegible] 100.

I. MAIN.

The recently reported breakthrough espial of gravitational waves emitted by coalescing binary black holes marked the starting point of the new field of gravitational wave astronomy [1]. The observations of Advanced LIGO gave evidence to a new population of black holes not consistent with our previous knowledge based on X-ray observations [2]. Increasing the low frequency sensitivity of current and future gravitational wave observatories will not only allow us to improve the signal-to-noise ratio with which we can observe them, but also allow us to extend the observation capability to even heavier binary black hole systems. This would allow us to shed light onto many important questions, such as: What is the precise astrophysical production route of binary black hole systems of tens of solar masses? What is the nature of spin-orbit and spin-spin couplings in coalescing binary black holes? Are the no-hair theorem and the second law of black hole mechanics valid?

In order to enhance the low frequency sensitivity of future gravitational wave detectors, a variety of noise sources has to be battled and improved, of which the most fundamental one is the so-called quantum noise, a inherent consequence of the quantum mechanics of the measurement process.

Quantum fluctuations of the electromagnetic field were identified as the main fundamental limitation to the sensitivity of electromagnetic weak force sensors in the late 60s by Braginsky [3]. He showed that continuous monitoring of the test object position to infer an external weak force (*e.g.*, GW) always leads to a quantum back-action of the meter on the probe object's position, thereby setting the *standard quantum limit* (SQL) on the achievable precision of such a measurement. In interferometric sensors, like GW interferometers, light is used to monitor the distances between the mirrors. Here back action noise originates from the quantum fluctuations of the light's intensity, leading to random radiation pressure forces acting on the mirrors. The corresponding additional displacement noise is most pronounced at low frequencies due to the mirrors' dynamical response and stems from the fundamental quantum fluctuations of the measurement apparatus. It comprises quantum fluctuations of the light's phase, setting the imprecision of the position monitoring $\Delta x_{\rm imp} \propto 1/\sqrt{N_{\rm ph}}$ (here $N_{\rm ph}$ is the number of photons used for measurement) and the back action noise ($\Delta x_{\rm BA} \propto \sqrt{N_{\rm ph}}$). Evidently, the naïve trade-off in $N_{\rm ph}$ yields the SQL that is the point where $\Delta x_{\rm imp} = \Delta x_{\rm BA}$.

It was almost immediately realised that the SQL is not a fundamental limitation, but rather a non-optimal choice of the observable to measure. Indeed the displacement operator of a suspended mirror with mass m and pendulum frequency Ω_m does not commute with itself at different times, $[\hat{x}(t),\, \hat{x}(t')] = i\hbar \sin[\Omega_m(t'-t)]/(m\Omega_m) \neq 0$ and therefore a displacement measurement at a time t will influence the result of of the one at a later time t'. The observables of the test object that commute at different times and thus can be monitored continuously with arbitrary precision are known as *quantum non-demolition (QND)* observables. The obvious choice for such observables are the conserved quantities of the test object, like energy, quadratures for the oscillator, or momentum for a free mass.

The idea of the quantum speed meter [4] was based

*Electronic address: shtefan.danilishin@ligo.org

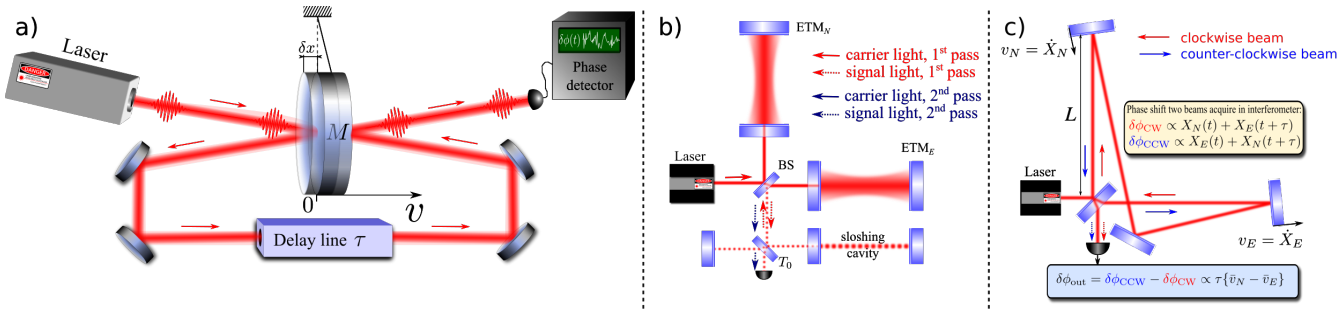

FIG. 1: [illegible]

on a premise that the relative velocity $\hat{v}$ of the interferometer mirrors on time-scales much shorter than the suspension oscillation period (so as one can view them as free masses) is proportional to the momentum, $\hat{p} = m\hat{v}$ which is conserved and thus is the QND observable. The more careful analysis has shown that the dynamics of the test object cannot be considered separately from that of the meter, which is the laser light in the case of GW interferometers. For a combined system 'mirrors+light', the generalised momentum is rather a sum of two terms, $\hat{P} = m\hat{v} - g_{\rm SM}(t)\hat{a}_c$ than a simple proportionality to velocity (see, *e.g.* Sec. 4.5.2 in [5]), where $g_{\rm SM}(t)$ is the strength of coupling between the light and the mirrors' mechanical motion, and $\hat{a}_c = (\hat{a} + \hat{a}^\dagger)/\sqrt{2}$ is the amplitude quadrature of light (defined in terms of photon annihilation (creation) operator $\hat{a}$ ($\hat{a}^\dagger$)). Nevertheless, not being a QND measurement in the strict sense, a speed measurement still provides a substantial reduction of random back-action force.

The simplest conceptual realisation of an optical speed meter is shown in Fig. 1a [6]. Here a laser sends short light pulses to the suspended mirror. The pulses, after reflecting off the front surface of the mirror are steered by auxiliary mirrors through the optical delay line with time constant τ towards the rear surface, where they encounter a second reflection before being measured at the phase measuring device. The information about the mirror's instantaneous position is written in each pulse's phase upon reflection. Hence, after two reflections the pulse's phase will be proportional to the mean velocity, $\bar{v}$, of the mirror in time τ: $\phi_{\rm pulse} \propto \hat{x}(t) - \hat{x}(t+\tau) \sim \tau\bar{v}$. Note that since the momentums transferred to the mirror by photons in the two reflections have opposite signs, and since there is no decoherence between the reflections, they compensate each other. Therefore quantum back-action noise is suppressed by $\sim \tau/T_{signal} \propto \Omega_{signal}\tau$, where $T_{signal} = 2\pi/\Omega_{signal}$ is the specific timescale of the signal force, *e.g.*, the period of GWs.

This example grasps the two key features, which the measurement scheme should possess to realise a speed measurement - (i) the probe (light) has to interact with the test object (mirror) twice, keeping coherence between the interactions (for coherent suppression of back-action noise), and (ii) the two terms in the interaction Hamiltonian that relate to the two consecutive measurements should have opposite signs.

The first interferometric implementation of such speed measurement suitable for detection of gravitational waves was proposed by Braginsky *et al.* in [7] (see Fig. 1b). Their idea was to modify the traditional Fabry-Pérot–Michelson scheme by adding an auxiliary "sloshing" optical cavity into the output port. This creates optically coupled cavities for the optical mode bearing the GW signal and makes this signal "slosh" back and forth between the cavities with alternating phase. Hence, after the second pass through the interferometer, the outgoing light bears exactly the required combination of position signals, $\propto \hat{x}(t) - \hat{x}(t+\tau) \sim \tau\bar{v}$, yielding the speed measurement. This scheme was nick-named a "sloshing speed meter". It has the distinctive feature that carrier and signal lights do not share the same optical path throughout the interaction, for the sloshing cavity is kept not pumped by a laser to preserve coherence of the signal light between the subsequent interactions with the main interferometer. This makes it very difficult to lock and control, and may also lead to signal loss from distortion in optical elements. A practical version of sloshing speed meter scheme was analysed in the great detail by Purdue and Chen in [8, 9].

Another solution was proposed by Chen in [10], demonstrating that a Sagnac interferometer with zero area performs a speed measurement. A simplified schematic of a zero-area Sagnac without arm cavities is shown in Fig. 1c and was analysed in [6]. Here the double measurement of the mirror position is performed naturally by two counter propagating light beams, which after the recombination on the beam splitter, produce the signal beam with phase dependent on the mean relative velocity of the end mirrors (see Fig. 1c).

Quantum back-action noise suppression in both schemes owes to the fact that the radiation pressure force component which drives differential displacement of the arm mirrors, $x_{\rm dARM} = x_n - x_e$, stems from the beat note of the carrier classical amplitude $A \propto \sqrt{P_c}$ (P_c is laser power circulating in the arms) with vacuum fields, $\hat{\boldsymbol{i}}$, entering the readout port of the interferometer rather

than with the laser fluctuations – $\hat{F}^{\rm b.a.}(t) \propto A\,\hat{i}_c(t)$, where $\hat{i}_c$ stands for amplitude quadrature amplitude of the input field $\hat{\boldsymbol{i}}$. In sloshing speed meters, subtraction of two back-action kicks is provided by the π-phase shift that the dark port field (bearing the signal sidebands and the vacuum fields) acquires after the reflection off the sloshing cavity, hence $\hat{F}^{\rm b.a.} \propto A\,\hat{i}_c(t) + e^{i\pi} A\,\hat{i}_c(t+\tau_{\rm sl}) = A\,(\hat{i}_c(t) - \hat{i}_c(t+\tau_{\rm sl}))$, and $\tau_{\rm sl}$ is the characterstic time of optical energy sloshing between the coupled cavities of the sloshing speed meter interferometer.

In the Sagnac interferometer, the very same π-phase shift arises naturally when the vacuum field $\hat{\boldsymbol{i}}$ gets split on a main beam splitter that introduces a π-phase difference between the transmitted and the reflected fields. Therefore, the quantum radiation pressure force created by the clockwise propagating beam on, say, the "east" mirror, $\hat{F}^{\rm b.a.}_{\rm CW,e} \propto A\,\hat{i}_c(t)$ is counter balanced by the one from the counter clockwise propagating beam, $\hat{F}^{\rm b.a.}_{\rm CCW,e} \propto -A\,\hat{i}_c(t+\tau_{\rm prop})$. Here $\tau_{\rm prop}$ stands for the time interval required for light to travel from one end mirror to another. Hence the partial cancellation of back action force.

As promising as the prospects of low-frequency sensitivity improvement with speed measurement might seem, those two schemes are rather complex to implement experimentally. The idea to simplify the speed meter setup by employing two orthogonal polarisations of light to separate the two beams sensing the mirrors in a Sagnac-type speed meter was first proposed by Danilishin [11] and then developed further by Wang *et al.* [12]. The proposed scheme of a polarisation Sagnac speed meter requires no modifications to the arm cavities, yet the input and output optics need substantial modifications and the implementation of additional polarising elements of large physical dimensions, not used inside the core interferometers of GW observatories so far.

The next step in simplifying speed meters, using polarisations was made by Wade *et al.* [13] who proposed to use the differential optical mode of the Michelson interferometer with the polarisation orthogonal to that of the pumping laser as an effective sloshing cavity. The polarisation separation of the signal light fields from the "sloshing" ones is achieved by means of two quarter wave plates (QWP), 2 mirrors and a polarisation beam splitter (PBS).

a. Polarisation circulation interferometer as speed meter: In this letter, we propose an even simpler scheme where the two orthogonal polarisation modes of the Michelson interferometer serve as two counter propagating beams of a Sagnac-type interferometer. The scheme is shown in Fig. 2. The main interferometer is pumped by the strong p-polarised laser field $\boldsymbol{p}_p$ that can be represented as a linear combination of two circularly polarised fields:

$$\boldsymbol{p}_p\vec{e}_p = \boldsymbol{p}_r\vec{e}_r + \boldsymbol{p}_l\vec{e}_l\,,\ |\boldsymbol{p}_r| = |\boldsymbol{p}_l| = |\boldsymbol{p}_p|/\sqrt{2}\,, \qquad (1)$$

where $\vec{e}_j$ $(j = \{p,\, r\,, l\})$ stand for polarisation basis vectors for p- and clockwise (r) and counter clockwise (l)

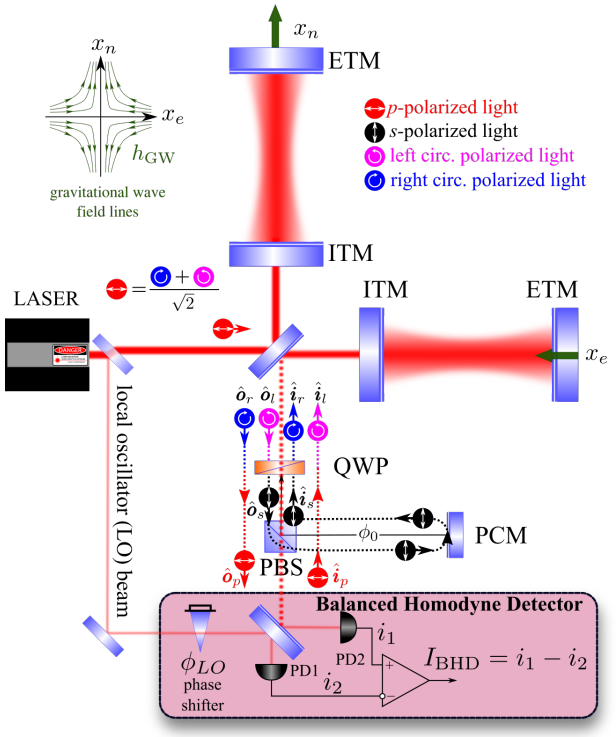

FIG. 2: Pl[illegible]

polarised light fields, respectively, and $|\boldsymbol{p}_j|$ stand for classical amplitudes of the respective fields.

Coherent coupling between the two polarisations is performed by the *polarisation circulator* comprising of quarter-wave plate, PBS and the closing highly reflective mirror. PBS and QWP define the new circular polarisation basis for the light modes of the interferometer. The PBS lets through the p-polarised vacuum field, $\hat{\boldsymbol{i}}_p$, that is transformed by the QWP into the l-polarised field $\hat{\boldsymbol{i}}_l$, which enters the Michelson interferometer from the dark port and interacts optomechanically with the $\boldsymbol{p}_l$ component of the pumping laser field $\boldsymbol{p}$ and the differential mechanical degree of freedom of the interferometer mirrors, $x_{\rm dARM}(t) = x_n(t) - x_e(t)$. The outgoing l-polarised field $\hat{\boldsymbol{o}}_l$, carrying information about the $x_{\rm dARM}$-displacement, is transformed into the s-polarised field $\hat{\boldsymbol{o}}_s$, which is reflected by the PBS towards the polarisation circulation mirror (PCM). The latter reflects $\hat{\boldsymbol{o}}_s$ back towards the PBS where it arrives with an acquired phase shift $2\phi_0 = \pi$ and enters the main interferometer as $\hat{\boldsymbol{i}}_r$ after being transformed by the QWP. There it interacts optomechanically once again, after the time delay defined by the arm cavities ring-down time τ, with the differential mechanical degree of freedom of the interferometer, $x_{\rm dARM}(t+\tau) = x_n(t+\tau) - x_e(t+\tau)$, and the $\boldsymbol{p}_r$ component of the pumping laser field $\boldsymbol{p}$.

The r-polarised output field $\hat{\boldsymbol{o}}_r$ finally leaves the dark port of the interferometer and is transformed by the

QWP into the p-polarised one, $\hat{\boldsymbol{o}}_p$. It is then transmitted by the PBS towards the balanced homodyne detector (BHD), where it is measured yielding the photocurrent, proportional to the differential speed of the arm mirrors:

$$I_{\rm BHD} \propto x_{\rm dARM}(t+\tau) - x_{\rm dARM}(t) \simeq \tau \bar{v}_{\rm dARM}(t)\,. \quad (2)$$

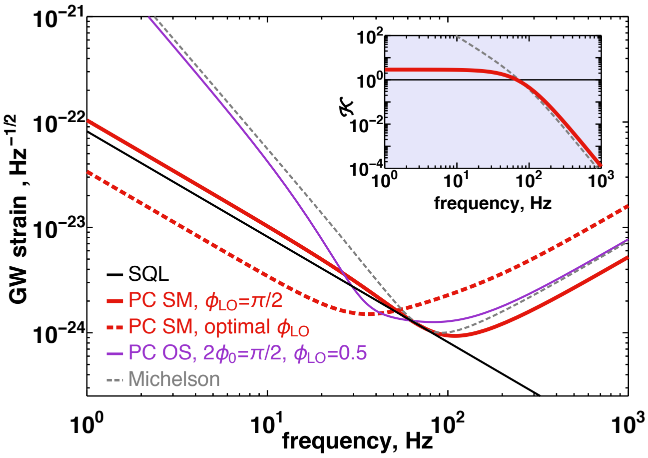

FIG. 3: Q[illegible] (QNLS) [illegible] (PC) [illegible] *red traces*) [illegible] QNLS [illegible] (*grey dashed trace*). *Red dashed curve* [illegible] SQL (*black trace*) [illegible] $\phi_{\rm LO} = \mathcal{K}_{\rm PCSM}(0)$. In [illegible] *phase readout, i.e.* $\phi_{\rm LO} = \pi/2$. *Purple trace* [illegible] QNLS [illegible] (2 [illegible] $\phi_0 = \pi/2$) [illegible] He [illegible] $M = 200$ kg [illegible] $P_c = 3$ MW [illegible] $\lambda_0 = 2\ \mu$m [illegible] $\gamma/2\pi = 80$ Hz

b. Quantum noise limited sensitivity. In order to give a more quantitative account of the quantum noise behaviour of the proposed scheme, we use the two-photon formalism of quantum optics [14] (see Methods for details). Quantum fluctuations of all the light fields of interest are represented by the pairs of quadrature amplitude operators formed in vectors, *e.g.* $\hat{\boldsymbol{i}} \equiv \{\hat{i}_c, \hat{i}_s\}^{\rm T}$, where $\hat{i}_{c,s}$ are *amplitude* and *phase* quadrature operators, respectively. Analysis of quantum noise of any interferometer starts from deriving the relations between the input and output light quadrature amplitudes, or *I/O-relations* for sideband fields at an off-set frequency $\Omega = \omega - \omega_p$. For the lossless interferometer tuned in resonance, so as the GW signal shows up in the phase quadrature only, the general shape of I/O-relations is very simple [15]:

$$\hat{o}_{p,c}(\Omega) = e^{2i\beta}\hat{i}_{p,c}(\Omega)\,, \quad (3)$$

$$\hat{o}_{p,s}(\Omega) = e^{2i\beta}\left[\hat{i}_{p,s}(\Omega) - \mathcal{K}\hat{i}_{p,c}(\Omega)\right] + e^{i\beta}\sqrt{2\mathcal{K}}\frac{h(\Omega)}{h_{\rm SQL}}\,, \quad (4)$$

where $\mathcal{K}(\Omega)$ is an optomechanical coupling factor describing the interaction of the mechanical degrees of freedom of the interferometer with light, $\beta(\Omega)$ is the frequency-dependent phase shift acquired by sideband fields as they pass through the interferometer, and $h_{\rm SQL} = \sqrt{\frac{8\hbar}{ML^2\Omega^2}}$ stands for the GW strain standard quantum limit for the effective mechanical mode of the interferometer with reduced mass M and arm lengths L. The second term in the brackets in (4) originates from the radiation pressure force driven by amplitude fluctuations. The last term in (4) describes the response of the interferometer to the GW signal with strain $h(\Omega) = 2x_{\rm dARM}(\Omega)/L$.

Using the matrix representation, outlined in the Methods, one can derive the quantum noise power spectral density (PSD) from the above I/O-relations that reads:

$$S^h(\Omega) = \frac{h^2_{\rm SQL}}{2}\left\{\frac{1 + [\mathcal{K} - \cot\phi_{\rm LO}]^2}{\mathcal{K}}\right\}, \quad (5)$$

where we assumed the homodyne readout of arbitrary quadrature defined by the local oscillator phase $\phi_{\rm LO}$. Note that the back-action term can be in principle made zero if $\cot\phi_{\rm LO} = \mathcal{K}$, which is however hard to achieve, for $\mathcal{K}$ is frequency dependent.

It is straightforward to derive the formulae for $\mathcal{K}$ and β for any tuned configuration of interferometer. For a Michelson interferometer with total circulating power in each arm P_c, laser frequency $\omega_p = 2\pi c/\lambda_p$ and effective half-bandwidth γ it reads $\mathcal{K}_{\rm MI} = \frac{2\Theta\gamma}{\Omega^2(\gamma^2+\Omega^2)}$ with $\Theta \equiv \frac{8\omega_p P_c}{McL}$, and frequency-dependent sidebands phase shift $\beta_{\rm MI} = \arctan\frac{\Omega}{\gamma}$. As shown in the Methods, the same expressions for the polarisation circulation interferometer in the speed meter regime reads:

$$\mathcal{K}_{\rm PCSM} = 2\mathcal{K}_{\rm MI}\sin^2\beta_{\rm MI} = \frac{4\Theta\gamma}{(\gamma^2+\Omega^2)^2}\,. \quad (6)$$

The behaviour of $\mathcal{K}$ as function of frequency reflects the strength of interaction of light at this particular sideband frequency Ω with the mirrors of the interferometer. This includes both, the strength of back-action and the level of response one can expect from the particular scheme at a given signal frequency, as reflected by two terms in (4) that contain $\mathcal{K}$. The inset to Fig. 3 shows clearly the differences between the Michelson and the PC speed meter in this regard. The sharp rise ($\propto \Omega^{-2}$) of $\mathcal{K}_{\rm MI}$ (grey trace) at low frequencies within the interferometer bandwidth, $\Omega < \gamma$, is responsible for worse quantum noise performance of the Michelson interferometer compared to the PC speed meter, characterised by the flat behaviour of $\mathcal{K}_{\rm PCSM}$ in that frequency region. This trend is responsible for the much improved speed meter quantum noise at low frequencies. Moreover, as $\mathcal{K}_{\rm PCSM}(\Omega \to 0) = const$, one can improve low frequency sensitivity of the speed meter even more by choosing to measure the optimal quadrature by tuning the homodyne angle to $\phi_{\rm LO} = {\rm arccot}\mathcal{K}_{\rm PCSM}(\Omega \to 0)$ as shown by the red dashed trace in Fig. 3.

In a simple special case of $\phi_{\rm LO} = \pi/2$ the QNLS PSD is $S^h(\Omega) = h^2_{\rm SQL}\left\{\mathcal{K} + \mathcal{K}^{-1}\right\}/2$, and one can clearly see that $\mathcal{K}(\Omega_q) = 1$ is the condition of reaching the SQL. It defines the frequency Ω_q, where QNLS curve touches the SQL, and therefore back-action and shot noise have equal contributions to the QNLS. For the Michelson interferometer, there is always a real solution to this condition, whereas for speed meter there is a threshold value of the ratio $\Theta/\gamma^3 \geq 1/4$ that sets the limit on the required circulating power for given interferometer bandwidth and *vice versa*. For given half-bandwidth γ, the circulating power, required for the PC speed meter to reach the SQL is $P_c \geq McL\gamma^3/(16\omega_p)$.

c. Optical spring in the PC speed meter: Noteworthy is the fact that depending on the tuning of the phase shift ϕ_0 the behaviour of the scheme varies in a wide range from a pure displacement meter for $2\phi_0 = 0$ to the speed meter corresponding to $2\phi_0 = \pi$. The intermediate values of the round-trip phase correspond to an interesting case of an optical spring, that is the emergence of a position-dependent restoring force on the test masses of the interferometer exerted by light. This effect, also known as *dynamical back-action*, is best understood on the example of $2\phi_0 = \pi/2$. In this case, the output field of the Michelson interferometer in l-polarisation mode carries the information about the arms differential displacement, $x_{\rm dARM}$, in the phase quadrature, $\hat{o}_{l,s} \propto x_{\rm dARM}$, whereas the amplitude quadrature, $\hat{o}_{l,c}$ contains purely amplitude fluctuations of the input field responsible for radiation pressure noise. After the round trip in the PC unit, the amplitude and the phase quadrature are swapped due to the $\pi/2$-phase shift, and the amplitude quadrature of the input field of the r-polarisation mode turns out to be dependent on the mirrors displacement, $\hat{i}_{r,c} \propto x_{\rm dARM}$. As a result, the differential radiation pressure force created by the beat note of this field with the carrier light will be proportional to the arms differential displacement, $F_l^{\rm b.a.} \propto |\boldsymbol{p}_r|\,\hat{i}_{r,c} \propto K x_{\rm dARM}$, thereby creating an effective *optical spring* with rigidity K.

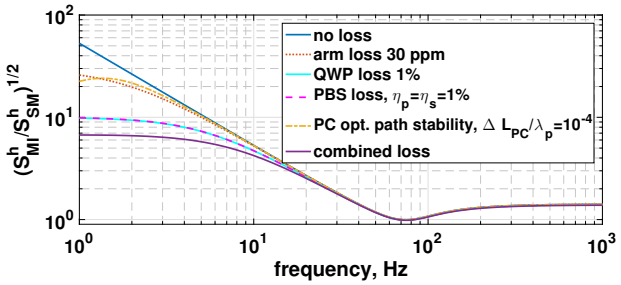

FIG. 4: If

d. Losses and imperfections analysis. To estimate the astrophysical potential of proposed scheme fairly, we need to assess the influence of the main sources of loss and imperfections of the real interferometer. In Fig 4, we show the relative contributions (normalised by the QNLS of the equivalent lossless Michelson interferometer) losses and imperfections make to the realistic QNLS.

The leading source of loss for the proposed scheme is photon absorption and loss in the polarisation components, *i.e.* absorption in the QWP (assumed single pass photon loss of $\epsilon_{\rm QWP} = 1\%$) and loss due to imperfect polarisation separation in the PBS (assumed extinction ratio for transmitted s-polarised and reflected p-polarised light of $\eta_s = \eta_p = 1\%$). One sees that both mechanisms contribute equally to the QNLS, which is no surprise as the input fields, $\hat{\boldsymbol{i}}_p$, pass both elements the same number of times (4) before being read out at the output as $\hat{\boldsymbol{o}}_p$. We also consider loss in the arm cavities, $\epsilon_{\rm arm} = 30$ ppm as a realistic projection for the next generation GW interferometers. The arm loss influence at low frequencies, as shown by Kimble *et al.*[15], amounts to additional incoherent back action noise created by loss-associated vacuum fields.

Finally, we analyse how robust the scheme is to the small deviations, $\Delta L_{\rm PC} \ll \lambda_p$, of the optical path length between the QWP and the PCM, that sets the value of ϕ_0. Deviations from the speed meter regime of $2\phi_0 = \pi$ results in a partial leakage of the back-action term from the sine quadrature into the cosine one, thereby creating an additional constant back-action force $\propto \sqrt{P_c}\Delta L_{\rm PC}/\lambda_p$ that leads, in conjunction with speed meter-like response ($\propto \Omega$), to a steep rise of noise at low frequencies, $\sqrt{S^h} \propto 1/\Omega^3$. This explains the downward bending of the corresponding yellow dash-dotted curve in Fig 4.

e. Astrophysics results and prospects: A quantitative comparison of the QNLS of our proposed speed meter scheme and QNLS of an equivalent Michelson interferom-

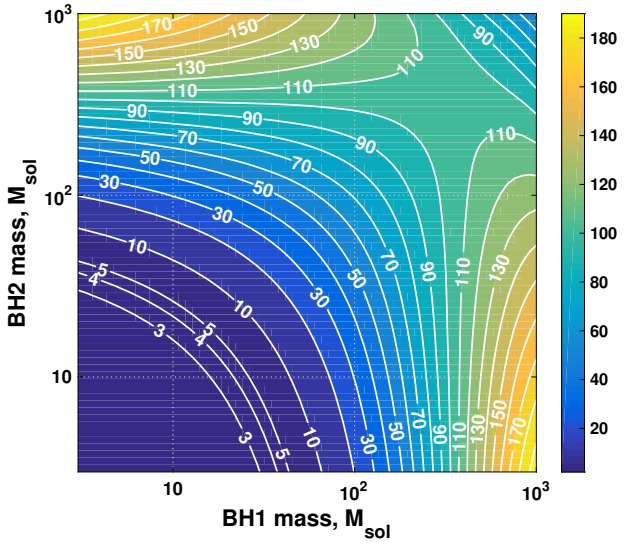

FIG. 5: I
QNLS (
QNLS (

eter is shown in Fig 5. (We assume for our analysis that due to the application of enhanced techniques all other noise sources, such as Newtonian noise [16], seismic noise [17] and suspension thermal noise [18], are pushed below the level of the QNLS). For this we consider the realistic speed meter including the optical losses shown in Fig 4 and calculate the corresponding inspiral range (integrated for frequencies between 1Hz and the last stable orbit), i.e. the distance up to which we can observe the BH coalescence before its signal to noise ratio decreases below 8. Then we compare the speed meter inspiral range to the insprial range of an equivalent Michelson interferometer and derive the plotted improvement factor in terms of event rate, assuming a homogeneous distribution throughout the Universe. We find for instance that for initial black hole masses similar to GW150914 [1] the speed meter would provide and improvement in the event rate of about 17. The largest improvement factors, however, are given for initial black holes in the range from $100 - 1000 M_\odot$ solar masses with obtained improvement factors larger than 100, which will open up access to investigating the potential existence of any BH population in this, so far unobserved, mass range.

f. Summary. In this article we suggested a new configuration for realising a quantum speed meter in laser-interferometric GW observatories. The key advantage of our configuration compared to other speed meter implementations, is that no additional optical components need to be implemented inside the main. The few additional components required to convert a standard advanced GW detector into our polarisation circulation speed meter can be placed in the output port of the interferometer (i.e. behind the signal extraction cavity). Our analysis showed that compared with a standard Fabry Perot Michelson interferometer our speed meter configuration provides significantly improved sensitivity at low frequencies. Further, a detailed investigation was carried out to identify the influence of imperfections on the sensitivity. We found that the most critical factor is the optical loss of the quarter wave plate and the PBS. Using realistic values for imperfections and loss we found that the speed meter QNLS sensitivity would yield and improvement factor of larger than 100 in event rate for binanry black hole mergers in the range from $10^2 - 10^3 M_\odot$. Future analyses will focus on investigating further sensitivity improvements from adding additional complementary quantum noise reduction techniques, such as the injection of squeezed light states.

g. Acknowledhgements. This work would not be possible without the support of and the insightful conversations with our colleagues from the Interferometry group of the Institute for Gravitational Research of the University of Glasgow. The authors are very grateful as well to our colleagues from the LIGO-Virgo Scientific Collaboration (LVC) for illuminating discussions and invaluable feedback on the research presented in this paper. SH, SLD, CG, JSH, and SS were supported by the European Research Council (ERC- 2012-StG: 307245). SLD and SH were supported by the Royal Society International Exchanges Scheme Grant IE160125. The work of EK and FYK was supported by the Russian Foundation for Basic Research Grants 14-02-00399 and 16-52-10069. FYK was also supported by the LIGO NSF Grant PHY-1305863. SS was supported by the European Commission Horizon 2020 Marie-Skodowska-Curie IF Actions, grant agreement 658366.

II. METHODS

h. Two-photon formalism: We calculate quantum noise of the proposed scheme using the so called two-photon formalism [14]. This formalism is best suited for steady state analysis of quantum fluctuations in the optomechanical devices. In this formalism, the electric field strain of the plane electromagnetic wave of the laser beam with frequency ω_p, cross-section area $\mathcal{A}$ and power $P_{\rm in}$ can be written as: $\hat{E}(t) = \mathcal{E}_0 \left[(A + \hat{a}_c(t)) \cos\omega_p t + \hat{a}_s(t) \sin\omega_p t\right]$, where $\mathcal{E}_0 = \sqrt{4\pi\hbar\omega_p/(\mathcal{A}c)}$ is the second quantisation normalising constant, $A = \sqrt{2P_{\rm in}/(\hbar\omega_p)}$ is the carrier dimensionless amplitude, and $\hat{a}_{c,s}(t)$ stand for *cosine* ("c") and *sine* ("s") quadrature amplitudes of the quantum fluctuations with zero mean.

i. Input-output relations of the interferometer: In steady state, it is more convenient to describe quantum fluctuations in frequency domain by introducing a signal sideband frequency $\Omega \to \omega - \omega_p$ centred around the laser frequency ω_p: $\hat{a}_{c,s}(t) = \int_{-\infty}^{\infty} \hat{a}_{c,s}(\Omega) e^{-i\Omega t} \frac{d\Omega}{2\pi}$. In this picture, any optomechanical interferometer can be characterised by a linear *input-output (I/O) relations* written as a linear vector transformation of the form:

$$\boldsymbol{b} = \mathbb{T}\boldsymbol{a} + \boldsymbol{t}\frac{h}{h_{\rm SQL}}, \text{ where } \mathbb{T} = \begin{bmatrix} T_{cc} & T_{cs} \\ T_{sc} & T_{ss} \end{bmatrix}, \ \boldsymbol{t} = \begin{bmatrix} t_c \\ t_s \end{bmatrix}, \quad (7)$$

where $\boldsymbol{a} = [\hat{a}_c(\Omega), \hat{a}_s(\Omega)]^{\rm T}$ and $\boldsymbol{b} = [\hat{b}_c(\Omega), \hat{b}_s(\Omega)]^{\rm T}$ are the 2-dimensional vectors of the input and the output light quadratures, respectively, $\mathbb{T}(\Omega)$ is a 2×2-matrix of the corresponding optical transfer matrices for the light fields, and $\boldsymbol{t}(\Omega)$ is a 2-dimensional vector of optomechanical response functions that characterises how GW with strain amplitude spectrum $h(\Omega)$ shows itself in the output quadratures of the light leaving the interferometer.

Readout photocurrent of the balanced homodyne detector is proportional to the quadrature of the outgoing light defined by the local oscillator phase angle ϕ_{LO}. Thus we can define the readout quadrature proportional to $\hat{I}_{\rm BHD}(\phi_{LO})$ as :

$$\hat{o}_{\phi_{LO}} \equiv \hat{b}_c \cos\phi_{LO} + \hat{b}_s \sin\phi_{LO} \equiv \mathbf{H}_{\phi_{LO}}^{\rm T} \cdot \boldsymbol{b}, \quad (8)$$

with $\mathbf{H}_{\phi_{LO}} \equiv \{\cos\phi_{LO}, \sin\phi_{LO}\}^{\rm T}$ and the spectral density of quantum noise at the output port of the interferometer can be obtained using the following simple rule:

$$S^h(\Omega) = h_{\rm SQL}^2 \frac{\mathbf{H}_{\phi_{LO}}^{\rm T} \cdot \mathbb{T} \cdot \mathbb{S}_a^{in} \cdot \mathbb{T}^\dagger \cdot \mathbf{H}_{\phi_{LO}}}{|\mathbf{H}_{\phi_{LO}}^{\rm T} \cdot \boldsymbol{t}_h|^2} \quad (9)$$

where $\mathbb{S}_a^{in}$ stands for spectral density matrix of injected light and components thereof can be defined as:

$$2\pi\delta(\Omega-\Omega')\,\mathbb{S}^{in}_{a,ij}(\Omega) \equiv \frac{1}{2}\langle in|\hat{a}_i(\Omega)(\hat{a}_j(\Omega'))^\dagger + (\hat{a}_j(\Omega'))^\dagger\hat{a}_i(\Omega)|in\rangle\,, \quad (10)$$

where $|in\rangle$ is the quantum state of vacuum injected in the dark port of the interferometer and $(i,j)=\{c,s\}$ (see Sec. 3.3 in [5] for more details). In present article we deal with *single-sided* spectral densities S and hence in case of input vacuum state:

$$|in\rangle = |vac\rangle \qquad \Rightarrow \qquad \mathbb{S}_a^{in} = \mathbb{I}\,.$$

j. I/O-relations of the polarisation circulation speed meter: The I/O-relations for our scheme can be obtained, using the Michelson interferometer I/O-relations twice, for each of the $\pm 45°$-polarisation modes. One just needs to keep in mind that both polarisations contribute to the common back-action force. The corresponding transfer matrix, $\mathbb{T}_{\rm MI}$ and response vector, $\boldsymbol{t}_{\rm MI}$, read:

$$\mathbb{T}_{\rm MI} = e^{2i\beta_{\rm MI}}\begin{bmatrix}0 & 1\\ -\mathcal{K}_{\rm MI} & 1\end{bmatrix},\ \boldsymbol{t}_{\rm MI} = e^{i\beta_{\rm MI}}\sqrt{2\mathcal{K}_{\rm MI}}\begin{bmatrix}0\\1\end{bmatrix}. \quad (11)$$

In the proposed scheme, both polarisation modes, $\boldsymbol{p}_l$ and $\boldsymbol{p}_r$, have half of the total circulating power provided by the pump laser. Therefore, each mode has only half of the full Michelson power and thus $\mathcal{K}_{r,l}\to\mathcal{K}_{\rm MI}/2$. Having this in mind, one can write down the I/O-relations for the two polarisation modes and for the link between them, provided by the PMC unit as:

$$\begin{cases}\hat{\boldsymbol{o}}_l &= \mathbb{T}^l_{\rm MI}\hat{\boldsymbol{i}}_l + \mathbb{T}^{\rm b.a.}_{\rm MI}\hat{\boldsymbol{i}}_r + \boldsymbol{t}_l\frac{h}{h_{\rm SQL}}\,,\\ \hat{\boldsymbol{o}}_r &= \mathbb{T}^{\rm b.a.}_{\rm MI}\hat{\boldsymbol{i}}_l + \mathbb{T}^r_{\rm MI}\hat{\boldsymbol{i}}_r + \boldsymbol{t}_r\frac{h}{h_{\rm SQL}}\,,\\ \hat{\boldsymbol{i}}_r &= \mathbb{P}^2_{\phi_0}\hat{\boldsymbol{o}}_l\,.\end{cases} \quad (12)$$

where $\mathbb{P}_{\phi_0} = \begin{bmatrix}\cos\phi_0 & -\sin\phi_0\\ \sin\phi_0 & \cos\phi_0\end{bmatrix}$ is the 2D rotation matrix by angle ϕ_0 that describes the phase shift carrier light acquires as it propagates from the QWP towards the PCM, and $\mathbb{T}^{\rm b.a.}_{\rm MI} = e^{2i\beta}\begin{bmatrix}0 & 0\\ -\mathcal{K}/2 & 0\end{bmatrix}$ is the back-action-only transfer matrix of the arm that accounts for the back-action effect on the corresponding polarisation mode created by the orthogonal mode radiation pressure.

Solving these equations for $\hat{\boldsymbol{o}}_r$, one gets for the new transfer matrix, $\mathbb{T}[\phi_0]$, and response function, $\boldsymbol{t}[\phi_0]$:

$$\mathbb{T}[\phi_0] = \mathbb{T}^{\rm b.a.}_{\rm MI} + \mathbb{T}^r_{\rm MI}\cdot\mathbb{P}^2_{\phi_0}\cdot\left[\mathbb{I}-\mathbb{T}^{\rm b.a.}_{\rm MI}\cdot\mathbb{P}^2_{\phi_0}\right]^{-1}\cdot\mathbb{T}^l_{\rm MI}\,,$$
$$\boldsymbol{t}[\phi_0] = \boldsymbol{t}_r + \mathbb{T}^r_{\rm MI}\cdot\mathbb{P}^2_{\phi_0}\cdot\left[\mathbb{I}-\mathbb{T}^{\rm b.a.}_{\rm MI}\cdot\mathbb{P}^2_{\phi_0}\right]^{-1}\cdot\boldsymbol{t}_l\,.$$

The speed meter regime of this interferometer is achieved when $2\phi_0 = \pi n$ for all integer n. In this case, one has:

$$\mathbb{T} = -e^{4i\beta}\begin{bmatrix}1 & 0\\ -2\mathcal{K}\sin^2\beta & 1\end{bmatrix} = e^{2i\beta_{\rm sag}}\begin{bmatrix}1 & 0\\ -\mathcal{K}_{\rm sag}/2 & 1\end{bmatrix} \quad (13)$$
$$\boldsymbol{t} = e^{2i\beta}\sqrt{\mathcal{K}}\begin{bmatrix}0\\ -2i\sin\beta\end{bmatrix} = e^{i\beta_{\rm sag}}\sqrt{\mathcal{K}_{\rm sag}}\begin{bmatrix}0\\1\end{bmatrix}, \quad (14)$$

where $\mathcal{K}_{\rm sag} = 4\mathcal{K}\sin^2\beta$ is the Sagnac speed meter OM coupling factor and $\beta_{\rm sag} = 2\beta+\pi/2$ is the corresponding phase shift for sidebands travelling through the Sagnac interferometer [10]. So we have shown that our scheme is equivalent to the Sagnac speed meter interferometer with 2 times lower input laser power. There is no surprise in that.

And finally, substituting (13) and (14) into Eq. (9), one gets the final expression for the PCSM quantum noise power spectral density in the form (5).

---

[1] B. P. Abbott *et al.*, Phys. Rev. Lett. **116**, 061102 (2016).
[2] B. P. Abbott *et al.*, Phys. Rev. X **6**, 041015 (2016).
[3] V. B. Braginsky, ... Soviet Journal of Experimental and Theoretical Physics **26**, 831 (1968).
[4] V. B. Braginsky and F. J. Khalili, Physics Letters A **147**, 251 (1990).
[5] S. L. Danilishin and F. Y. Khalili, Living Reviews in Relativity **15**, 5 (2012).
[6] S. Danilishin, Optics and Spectroscopy **96**, 727 (2004), 3rd Digital Kyoto ... Moscow ... MOSCOW, RUSSIA, MAY 26-28, 2003.
[7] V. B. Braginsky, M. L. Gorodetsky, F. Y. Khalili, and K. S. Thorne, Phys. Rev. D **61**, 044002 (2000).
[8] P. Purdue, Phys. Rev. D **66**, 022001 (2002).
[9] P. Purdue and Y. Chen, Phys. Rev. D **66**, 122004 (2002).
[10] Y. Chen, Phys. Rev. D **67**, 122004 (2003).
[11] S. L. Danilishin, Phys. Rev. D **69**, 102003 (2004).
[12] M. Wang *et al.*, Phys. Rev. D **87**, 096008 (2013).
[13] A. R. Wade *et al.*, Phys. Rev. D **86**, 062001 (2012).
[14] C. Caves and B. Schumaker, Phys. Rev. A **31**, 30683092 (1985).
[15] H. Kimble, Y. Levin, A. Matsko, K. Thorne, and S. Vyatchanin, Phys. Rev. D **65**, 022002 (2002).
[16] P. R. Saulson, Phys. Rev. D **30**, 732 (1984).
[17] F. Matichard *et al.*, Classical and Quantum Gravity **32**, 185003 (2015).
[18] A. V. Cumming *et al.*, Classical and Quantum Gravity **29**, 035003 (2012).